Microtubule dynamics regulates mitochondrial fission

Kritika Mehta[1], Manjyot Kaur Chug[1], Siddharth Jhunjhunwala[1] and Vaishnavi Ananthanarayanan[1,*]

[1] *Centre for BioSystems Science and Engineering, Indian Institute of Science, Bangalore 560012*

** To whom correspondence may be addressed. Email: vaish@be.iisc.ernet.in*

Mitochondria are organised as tubular networks in the cell and undergo fission and fusion. Equilibrium between the fission and fusion events is necessary to maintain normal mitochondrial function, with dysfunction of these dynamic processes correlated with disease states including neurodegeneration[1,2], cancer[3], and cardiomyopathy[4]. While several of the molecular players involved in mediating the dynamics of mitochondria have been identified[5], the precise cellular cues that initiate fission or fusion remain unknown. In fission yeast, as in mammalian cells, mitochondrial positioning and partitioning are microtubule-mediated[6,7]. In interphase, fission yeast mitochondria associate with microtubule bundles that are aligned along the long axis of the cell[8]. Here we show that perturbation of microtubule dynamics via kinesin-like proteins is sufficient to shift the balance between fission and fusion of mitochondria and consequently, change mitochondrial morphology. Our results additionally fit with a stochastic model for partitioning of mitochondria during closed mitosis in fission yeast, with the absence of cytoplasmic microtubules providing the basis for increased mitochondrial fission. Finally, we propose a model whereby association of mitochondria with microtubules inhibits proper assembly of the dynamin GTPase-related fission protein Dnm1 around mitochondria. Thus, we demonstrate a general mechanism by which mitochondrial dynamics may be dictated by the dynamics of the microtubule cytoskeleton.

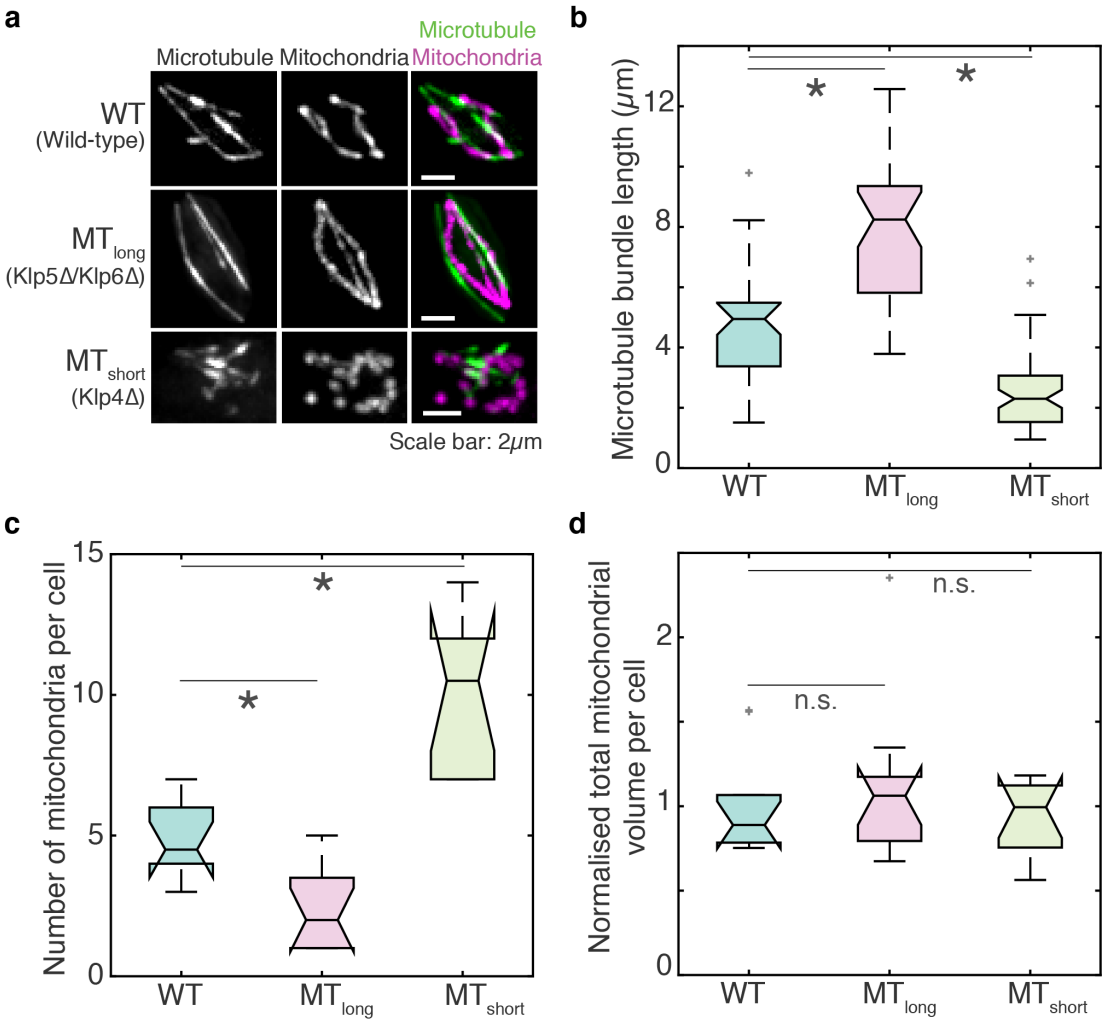

Figure 1. Mitochondrial number is inversely proportional to microtubule length. a, Maximum intensity projections of deconvolved Z-stack images of microtubules (left), mitochondria (centre) and their composite (right) in wild-type ('WT', top, strain KI001, see Table S1), Klp5Δ/Klp6Δ ('MT_{long}', strain G3B, see Table S1) and Klp4Δ ('MT_{short}', strain G5B, see Table S1) cells. **b,** Box plot of length of anti-parallel microtubule bundles in WT, MT_{long} and MT_{short} cells (*n*=40, 37 and 63 bundles respectively). **c,** Box plot of number of mitochondria per cell in WT, MT_{long} and MT_{short} cells (*n*=10, 12 and 13 cells respectively). **d,** Box plot of the total volume of mitochondria per cell in WT, MT_{long} and MT_{short} cells normalised to mean total wild-type mitochondrial volume (*n*=10, 12 and 13 cells respectively). Light grey crosses represent outliers, asterisk represents significance ($p<0.05$) and 'n.s.' indicates no significant difference.

The fission yeast protein Mmb1 has been identified to associate mitochondria with dynamic microtubules[9]. Upon microtubule depolymerisation using methyl benzimidazol-2-yl-carbamate (MBC, see Supplementary Information) or deletion of Mmb1, mitochondria have been observed to undergo rapid fragmentation[9–11]. We observed that mitochondria did indeed undergo increased fission in the absence of microtubules, but did not subsequently aggregate as reported previously (Extended Data Fig. 1a-c). Instead the fragmented

mitochondria were mobile and frequently in close contact with each other (Extended Data Fig. 1b, c, Supplementary Video S1). Since the depolymerisation of microtubules had a direct effect on mitochondrial fission, we set out to study the consequence of modification of microtubule dynamics on mitochondrial dynamics. To this end, we visualised the mitochondria and microtubules of fission yeast strains carrying deletions of antagonistic kinesin-like proteins, Klp5/Klp6 and Klp4 in high-resolution deconvolved images (Fig. 1a, Supplementary Videos S2, S3 and S4).

The heteromeric Klp5/Klp6 motor is required for maintenance of interphase microtubule length by promoting catastrophe at microtubule plus ends[12,13]. Cells lacking Klp5 and Klp6 exhibited long microtubules ('MT_{long}', Fig. 1b) as reported previously due to a decreased catastrophe rate[12]. Klp4 is required for polarised growth in fission yeast and has been suggested to promote microtubule growth[14,15]. As a result, in the absence of Klp4, microtubule anti-parallel bundles were only half the length of wild-type bundles ('MT_{short}', Fig. 1b). As in wild-type cells, mitochondria in Klp5Δ/Klp6Δ were in close contact with the microtubule, whereas we observed reduced association between the short microtubules and mitochondria of Klp4Δ cells (Fig. 1a, Supplementary Videos S3 and S4). While wild-type cells had 4-5 mitochondria per cell, we observed that Klp5Δ/Klp6Δ contained only ~2. In contrast, Klp4Δ cells had 10 mitochondria per cell on an average (Fig. 1c). This indicated that the number of mitochondria per cell was inversely related to the length of microtubule bundle. So too, cells carrying a deletion of the EB1 homologue Mal3 also produced small microtubule bundles[16] and additionally contained several mitochondria as reported previously[9] (Extended Data Fig. 1d). However, the decrease in the number of mitochondria in Klp5Δ/Klp6Δ cells and increase in Klp4Δ cells were not at the expense of mitochondrial volume, since the net mitochondrial volume in both cases was comparable to wild-type mitochondrial volume (Fig. 1d, Extended Data Fig. 1e).

To understand the difference in mitochondrial numbers in wild-type, Klp5Δ/Klp6Δ and Klp4Δ cells, we acquired and analysed time-lapse videos at the single mitochondrion level in all three cases (Fig. 2a, Supplementary Videos S5, S6 and S7). Similar to our observations from high-resolution images, we measured ~5, ~2 and ~8 mitochondria on an average in wild-type, Klp5Δ/Klp6Δ and Klp4Δ cells respectively (Fig. 1c and 2b). Analysis of evolution of these mitochondrial numbers revealed no significant changes with time (Fig. 2b). Interestingly, we discovered that the size of the individual mitochondrion correlated with

the length of the microtubule bundle in the cell, with Klp5Δ/Klp6Δ cells containing the longest mitochondria and Klp4Δ cells having short mitochondria. Wild-type cells predictably exhibited mitochondrial size ranges that lay between that of Klp5Δ/Klp6Δ and Klp4Δ cells (Fig. 2c, Extended Data Fig. 2a-c).

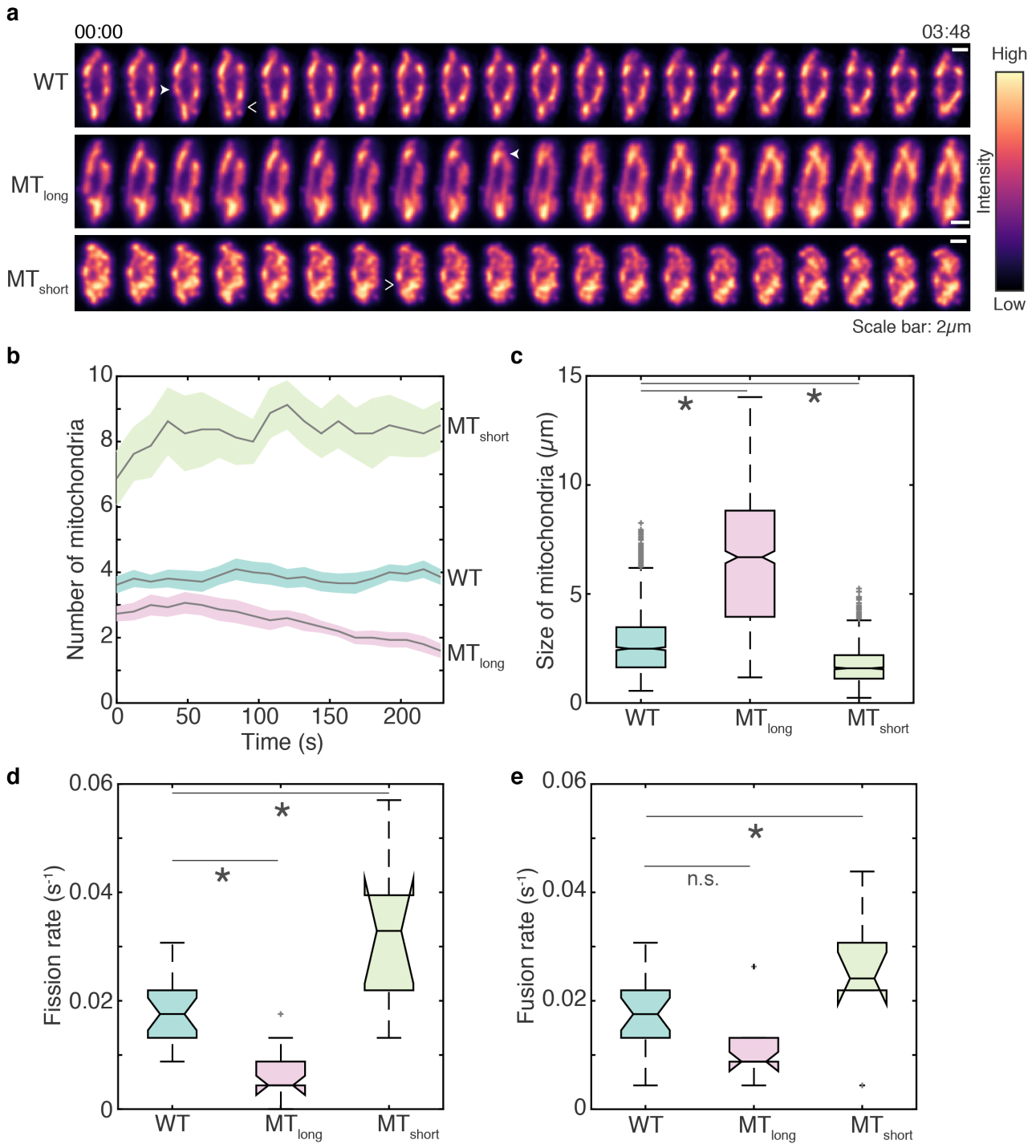

Figure 2. Microtubule catastrophe rate determines fission rate of mitochondria. a, Montage of maximum intensity projected confocal Z-stack images of wild-type ('WT', strain KI001, see Table S1), Klp5Δ/Klp6Δ ('MT_{long}', strain G3B, see Table S1) and Klp4Δ ('MT_{short}', strain G5B, see Table S1) cells represented in the intensity map indicated to the

right of the images. White solid arrowheads point to representative fusion events and open arrowheads to fission events. Time is indicated above the images in mm:ss. **b,** Evolution of mitochondrial number with time indicated as mean (solid grey line) and standard error of the mean (shaded region) for WT, MT_{long} and MT_{short} cells (*n*=21, 15 and 8 cells respectively). **c,** Box plot of the size of mitochondria in WT, MT_{long} and MT_{short} cells, calculated as the length of the major axis of an ellipse fitted to each mitochondrion (*n*=1613, 739 and 1326 mitochondria respectively). **d,** Box plot of the fission rate of mitochondria per second in WT, MT_{long} and MT_{short} cells (*n*=21, 15 and 8 cells respectively). **e,** Box plot of the fusion rate of mitochondria per second in WT, MT_{long} and MT_{short} cells (*n*=21, 15 and 8 cells respectively). Light grey crosses represent outliers, asterisk represents significance ($p<0.05$) and 'n.s.' indicates no significant difference.

Additionally, mitochondria in wild-type cells underwent ~1 fission and ~1 fusion event every minute on an average, whereas Klp5Δ/Klp6Δ cells exhibited a fission rate that was half that of wild-type, and Klp4Δ mitochondria had a fission rate that was almost double that of (Fig. 2d). The fusion rate of mitochondria in Klp4Δ cells was slightly higher than in wild-type and Klp5Δ/Klp6Δ cells (Fig. 2e), likely due to the increased number of mitochondria in Klp4Δ cells that could participate in fusion. However, the resulting ratio of the mean fission rate to the mean fusion rate was ~1, ~0.5 and ~1.3 in wild-type, Klp5Δ/Klp6Δ and Klp4Δ cells respectively. We therefore concluded that the difference in mitochondrial numbers between wild-type cells and Klp5Δ/Klp6Δ and Klp4Δ arose primarily due to the changes in fission rates of mitochondria. Increase in oxidative stress via reactive oxygen species (ROS) levels has also been described to induce mitochondrial fission[17]. However, we measured no difference in ROS levels between wild-type, Klp5Δ/Klp6Δ, and Klp4Δ cells (Extended Data Fig. 2d).

To test the role of the microtubule in determining the length and dynamics of mitochondria, we depolymerised microtubules in wild-type and Klp5Δ/Klp6Δ cells and visualised the mitochondria in time-lapse movies (Extended Data Fig. 3a). In both cases, upon microtubule depolymerisation, we observed a switch in mitochondrial morphology to increased numbers, increased fission and unaltered fusion rate that was reminiscent of Klp4Δ cells (Extended Data Fig. 3b-h).

Fission yeast undergoes closed mitosis, wherein the nuclear envelope does not undergo breakdown during cell division[18]. Upon onset of mitosis in fission yeast, the interphase microtubules that were previously in the cytoplasm are reorganised to form the spindle inside the closed nucleus. This natural situation mimics the depolymerisation of microtubules via the chemical inhibitor MBC. Therefore, we set out to study the changes in

the mitochondrial network upon cell entry into mitosis. We first obtained high-resolution deconvolved images of the microtubule and mitochondria in fission yeast cells undergoing cell division (Fig. 3a, Extended Data Fig. 4a, Supplementary Video S8). We observed that dividing wild-type cells had ~4x the number of mitochondria in interphase cells (Fig. 3b). Moreover, similar to what was seen in cells lacking microtubules or Klp4 (Fig. 1a), mitochondria in dividing cells were shorter and more rounded (Fig. 3a, Extended Data Fig. 4a). There was no relationship between length of the mitotic spindle and the number of mitochondria (Fig. 3b, Extended Data Fig. 4a), indicating that the increased fission likely occurred fairly early upon entry into mitosis. Analysis of time-lapse videos of wild-type cells before and 10min after entry into mitosis revealed a doubling of mitochondrial numbers in this time (Fig. 3c, d, Supplementary Video S9). Note that this is likely an underestimate since we were unable to reliably resolve some of the mitochondria in these lower-resolution images. In this same period of time, non-dividing interphase cells did not show any change in mitochondrial numbers (Extended Data Fig. 4b, c).

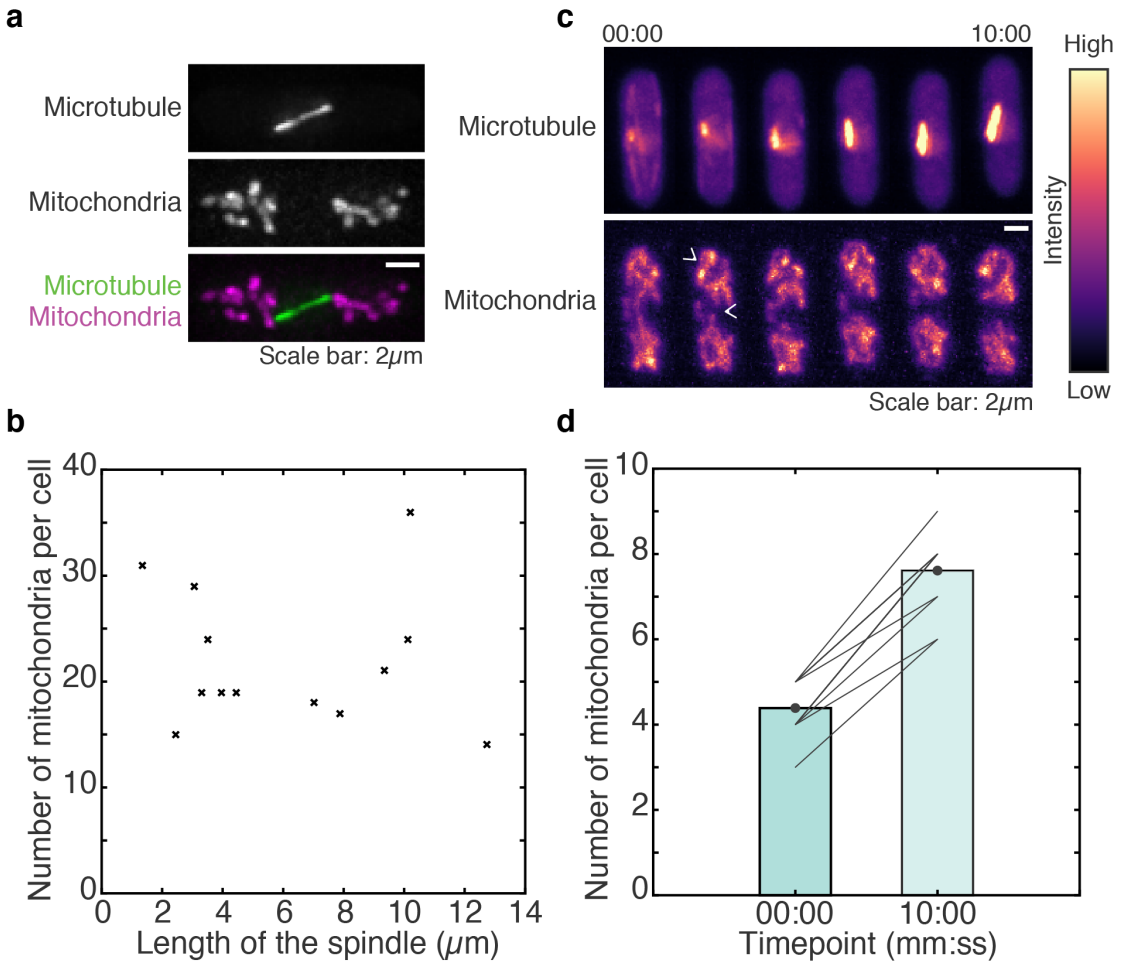

Figure 3. Mitotic cells contain several short mitochondria. a, Maximum intensity projections of deconvolved Z-stack images of the microtubules (top), mitochondria (centre) and their composite (bottom) of a wild-type cell (strain KI001, see Table S1) undergoing division. **b,** Scatter plot of the length of the mitotic spindle vs. the number of mitochondria per cell in dividing cells (*n*=13 cells). **c,** Montage of maximum intensity projected confocal Z-stack images of the microtubules (top) and mitochondria (bottom) in a wild-type cell (strain KI001, see Table S1) undergoing cell division represented in the intensity map indicated to the right of the images. White open arrowheads point to representative fission events. Time is indicated above the images in mm:ss. **d,** Bar plot of the mean number of mitochondria per cell before ('00:00') and 10mins after ('10:00') the onset of mitosis. Solid grey lines represent data from individual cells (*n*=16 cells).

Taken together, our results suggest that mitochondrial fission is inhibited by the association of mitochondria with microtubules. The mitochondrial outer-membrane fission protein in yeast is the dynamin-related GTPase, Dnm1[10]. Dnm1 brings about the fission of mitochondria by self-assembling into a ring around the diameter of the mitochondria and employing its GTPase activity to effect the scission[19]. In the absence of Dnm1, mitochondria are organised as extended, fused 'nets'[10,20]. We hypothesised that the binding of mitochondria to microtubules physically hinders the formation of a complete ring of Dnm1 around the mitochondrion. To test this hypothesis, we introduced GFP-tagged Dnm1 under the control of the thiamine-repressible nmt1 promoter[21] into wild-type cells expressing fluorescent microtubules (see Table S1). C- or N-terminal tagging of Dnm1 renders it inactive[10] and therefore the scission activity of Dnm1 could not be directly observed (Extended Data Fig. 5a). However, we visualised the localisation of Dnm1 'spots', representing Dnm1 assembly, with respect to microtubules. Although almost 100% of the Dnm1 spots colocalised with mitochondria (Extended Data Fig. 5a), 85% of the spots did not localise on the microtubule (Fig. 4a, Supplementary Video S10), indicating that the presence of microtubule had an inhibitory effect on the assembly of the Dnm1 ring. Moreover, we counted a slight decrease in Dnm1 spots in Klp5Δ/Klp6Δ, and ~2x increase in Klp4Δ cells as compared to wild-type cells (Extended Data Fig. 5b), corroborating our previous observations indicating decreased fission in the former and increased fission in the latter (Fig. 2d).

We discovered that microtubule dynamics is a strong determinant for mitochondrial dynamics and thereby, morphology (Extended Data Fig. 5c). Mitochondrial fission rate was proportional to microtubule catastrophe rate, whereas the fusion rate was almost completely insensitive to microtubule dynamics (Extended Data Fig. 5c). While previous studies

discounted the role of motors in the determination of mitochondrial positioning in fission yeast[11,22–24], we have identified kinesin-like proteins that regulate mitochondrial morphology through their control over microtubule length.

We propose that equilibrium between fission and fusion of mitochondria in interphase cells can be maintained solely by the inherent dynamic instability of microtubules. Perturbation of microtubule dynamics shifts the balance between fission and fusion rates to a different set point, leading to modification of mitochondrial numbers and morphology. Fission yeast cells likely employ this strategy to fragment interphase mitochondria by emptying the cytoplasm of its microtubules upon onset of mitosis, thereby ensuring stochastic[25] albeit equal partitioning of the several small mitochondria between future daughter cells (Fig. 4b).

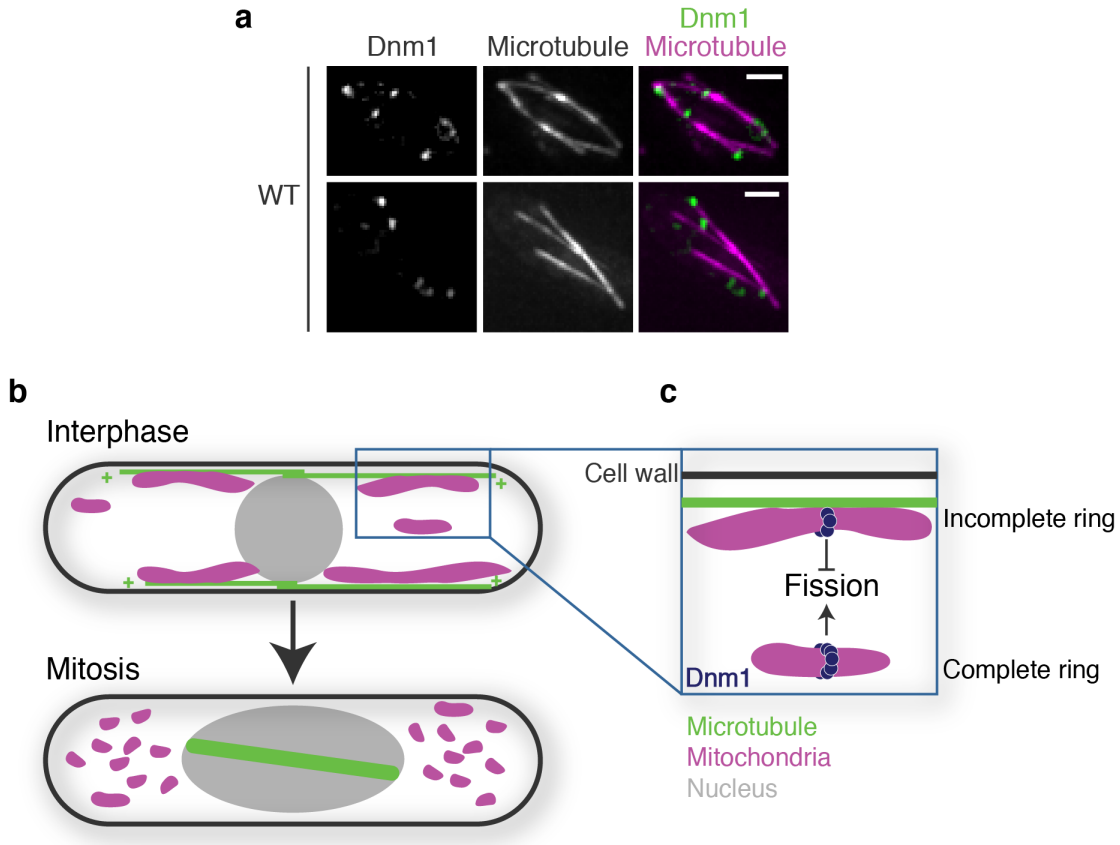

Figure 4. Dnm1 spots occur in locations devoid of the microtubule. a, Maximum intensity projections of deconvolved Z-stack images of Dnm1 (left), microtubules (centre) and their composite (right) in wild-type cells expressing fluorescent Dnm1 and tubulin (strain MTY271 transformed with pREP41-Dnm1-Cterm-GFP, see Table S1). A majority of Dnm1 spots did not localise on the microtubule (*n*=14 cells) **b,** Model of mitochondrial dynamics mediated by microtubule dynamics. Microtubules polymerise and depolymerise at their plus ends ('+'). Absence of microtubule bundles in the cytoplasm during cell division enables the fragmentation of mitochondria. **c,** When mitochondria are bound to

microtubules, Dnm1 ring assembly might be inhibited. Upon microtubule depolymerisation, this inhibition is alleviated and Dnm1 can effectively mediate scission of mitochondria.

We observed that Dnm1 spots were excluded from microtubules (Fig. 4a). We also propose the failure of Dnm1 ring assembly in the presence of microtubules as the nexus between microtubule dynamics and mitochondrial dynamics (Fig. 4c). Whether the microtubule is a simple physical impediment to the formation and activity of the Dnm1 ring or a more complicated chemical inhibitor would be the focus of future studies.

Destabilisation of microtubules is a hallmark of several neurodegenerative disorders including Alzheimer's, Parkinson's and Huntington's disease[26]. So too, colorectal cancer has been characterised by the absence of the tumour suppressor gene APC, which also modulates microtubule dynamics[27]. Remarkably, all these disease states have also been correlated with dysfunction of mitochondrial dynamics[28,29]. In future, it would be interesting to investigate the effect of restoration of microtubule dynamics on the mitochondrial fission and fusion in these scenarios, and consequently on the disease states.

METHODS

Methods are presented in the Supplementary Information.

1. Hirai, K. *et al.* Mitochondrial abnormalities in Alzheimer's disease. *J. Neurosci.* **21,** 3017–23 (2001).
2. Deng, H., Dodson, M. W., Huang, H. & Guo, M. The Parkinson's disease genes pink1 and parkin promote mitochondrial fission and/or inhibit fusion in Drosophila. *Proc. Natl. Acad. Sci.* **105,** 14503–14508 (2008).
3. Graves, J. A. *et al.* Mitochondrial Structure, Function and Dynamics Are Temporally Controlled by c-Myc. *PLoS One* **7,** e37699 (2012).
4. Ashrafian, H. *et al.* A Mutation in the Mitochondrial Fission Gene Dnm1l Leads to Cardiomyopathy. *PLoS Genet.* **6,** e1001000 (2010).
5. Westermann, B. Molecular machinery of mitochondrial fusion and fission. *J. Biol. Chem.* **283,** 13501–5 (2008).
6. Boldogh, I. R. & Pon, L. A. Mitochondria on the move. *Trends Cell Biol.* **17,** 502–10 (2007).
7. Yaffe, M. *et al.* Microtubules mediate mitochondrial distribution in fission yeast. *Proc.*

Natl. Acad. Sci. **93,** 11664–11668 (1996).

8. Höög, J. L. *et al.* Organization of interphase microtubules in fission yeast analyzed by electron tomography. *Dev. Cell* **12,** 349–61 (2007).
9. Fu, C., Jain, D., Costa, J., Velve-Casquillas, G. & Tran, P. T. Mmb1p binds mitochondria to dynamic microtubules. *Curr. Biol.* **21,** 1431–1439 (2011).
10. Jourdain, I., Gachet, Y. & Hyams, J. S. The dynamin related protein Dnm1 fragments mitochondria in a microtubule-dependent manner during the fission yeast cell cycle. *Cell Motil. Cytoskeleton* **66,** 509–523 (2009).
11. Li, T., Zheng, F., Cheung, M., Wang, F. & Fu, C. Fission yeast mitochondria are distributed by dynamic microtubules in a motor-independent manner. *Sci. Rep.* **5,** 11023 (2015).
12. Tischer, C., Brunner, D. & Dogterom, M. Force- and kinesin-8-dependent effects in the spatial regulation of fission yeast microtubule dynamics. *Mol. Syst. Biol.* **5,** 250 (2009).
13. West, R. R., Malmstrom, T., Troxell, C. L. & McIntosh, J. R. Two related kinesins, klp5+ and klp6+, foster microtubule disassembly and are required for meiosis in fission yeast. *Mol. Biol. Cell* **12,** 3919–32 (2001).
14. Browning, H. *et al.* Tea2p is a kinesin-like protein required to generate polarized growth in fission yeast. *J. Cell Biol.* **151,** 15–28 (2000).
15. Busch, K. E., Hayles, J., Nurse, P. & Brunner, D. Tea2p Kinesin Is Involved in Spatial Microtubule Organization by Transporting Tip1p on Microtubules. *Dev. Cell* **6,** 831–843 (2004).
16. Beinhauer, J. D., Hagan, I. M., Hegemann, J. H. & Fleig, U. Mal3, the fission yeast homologue of the human APC-interacting protein EB-1 is required for microtubule integrity and the maintenance of cell form. *J. Cell Biol.* **139,** 717–28 (1997).
17. Pletjushkina, O. Y. *et al.* Effect of oxidative stress on dynamics of mitochondrial reticulum. *Biochim. Biophys. Acta - Bioenerg.* **1757,** 518–524 (2006).
18. Ding, R., West, R. R., Morphew, D. M., Oakley, B. R. & McIntosh, J. R. The spindle pole body of Schizosaccharomyces pombe enters and leaves the nuclear envelope as the cell cycle proceeds. *Mol. Biol. Cell* **8,** 1461–79 (1997).
19. Ingerman, E. *et al.* Dnm1 forms spirals that are structurally tailored to fit mitochondria. *J. Cell Biol.* **170,** 1021–7 (2005).

20. Guillou, E., Bousquet, C., Daloyau, M., Emorine, L. J. & Belenguer, P. Msp1p is an intermembrane space dynamin-related protein that mediates mitochondrial fusion in a Dnm1p-dependent manner in S. pombe. *FEBS Lett.* **579,** 1109–16 (2005).
21. Maundrell, K. nmt1 of fission yeast. A highly transcribed gene completely repressed by thiamine. *J. Biol. Chem.* **265,** 10857–64 (1990).
22. Brazer, S. W., Williams, H. P. & Chappell, T. G. A fission yeast kinesin affects Golgi membrane recycling. 149–166 (2000).
23. Yaffe, M. P., Stuurman, N. & Vale, R. D. Mitochondrial positioning in fission yeast is driven by association with dynamic microtubules and mitotic spindle poles. *PNAS* **100,** 11424–11428 (2003).
24. Chiron, S., Bobkova, A., Zhou, H. & Yaffe, M. P. CLASP regulates mitochondrial distribution in Schizosaccharomyces pombe. *J. Cell Biol.* **182,** 41–49 (2008).
25. Birky, C. W. The partitioning of cytoplasmic organelles at cell division. *Int. Rev. Cytol. Suppl.* **15,** 49–89 (1983).
26. Dubey, J., Ratnakaran, N. & Koushika, S. P. Neurodegeneration and microtubule dynamics: death by a thousand cuts. *Front. Cell. Neurosci.* **9,** 343 (2015).
27. Kroboth, K. *et al.* Lack of Adenomatous Polyposis Coli Protein Correlates with a Decrease in Cell Migration and Overall Changes in Microtubule Stability. *Mol. Biol. Cell* **18,** 910–918 (2007).
28. Chen, H. & Chan, D. C. Mitochondrial dynamics--fusion, fission, movement, and mitophagy--in neurodegenerative diseases. *Hum. Mol. Genet.* **18,** R169-76 (2009).
29. Senft, D. & Ronai, Z. A. Regulators of mitochondrial dynamics in cancer. *Curr. Opin. Cell Biol.* **39,** 43–52 (2016).

ACKNOWLEDGEMENTS

We thank J. M. Thankachan, S. S. Nuthalapati and M. Ayushman for pilot experiments; High Content Imaging Facility at BSSE, IISc, and P. I. Rajyaguru for the use of the InCell 6000, and Deltavision RT microscopes respectively; P. Delivani, I. Jourdain, R.C. Salas, M. Takaine, I. Tolic, P. Tran, and NBRP Japan for yeast strains and constructs; S. Jain for CellROX reagent. The research was supported by the Department of Science and Technology (India)-INSPIRE Faculty Award, the Department of Biotechnology (India) Innovative Young Biotechnologist Award, and the Science and Engineering Research

Board (SERB, India) Early Career Research Award awarded to V.A., and SERB Early Career Research Award awarded to S.J.

AUTHOR CONTRIBUTIONS

K.M. carried out the Dnm1 experiments, M.K.C. and S. J. carried out and analysed the flow cytometry experiments, V.A. performed all the other experiments and data analysis, designed the project, and wrote the paper.

COMPETING FINANCIAL INTERESTS

The authors declare no competing financial interests.

Extended Data

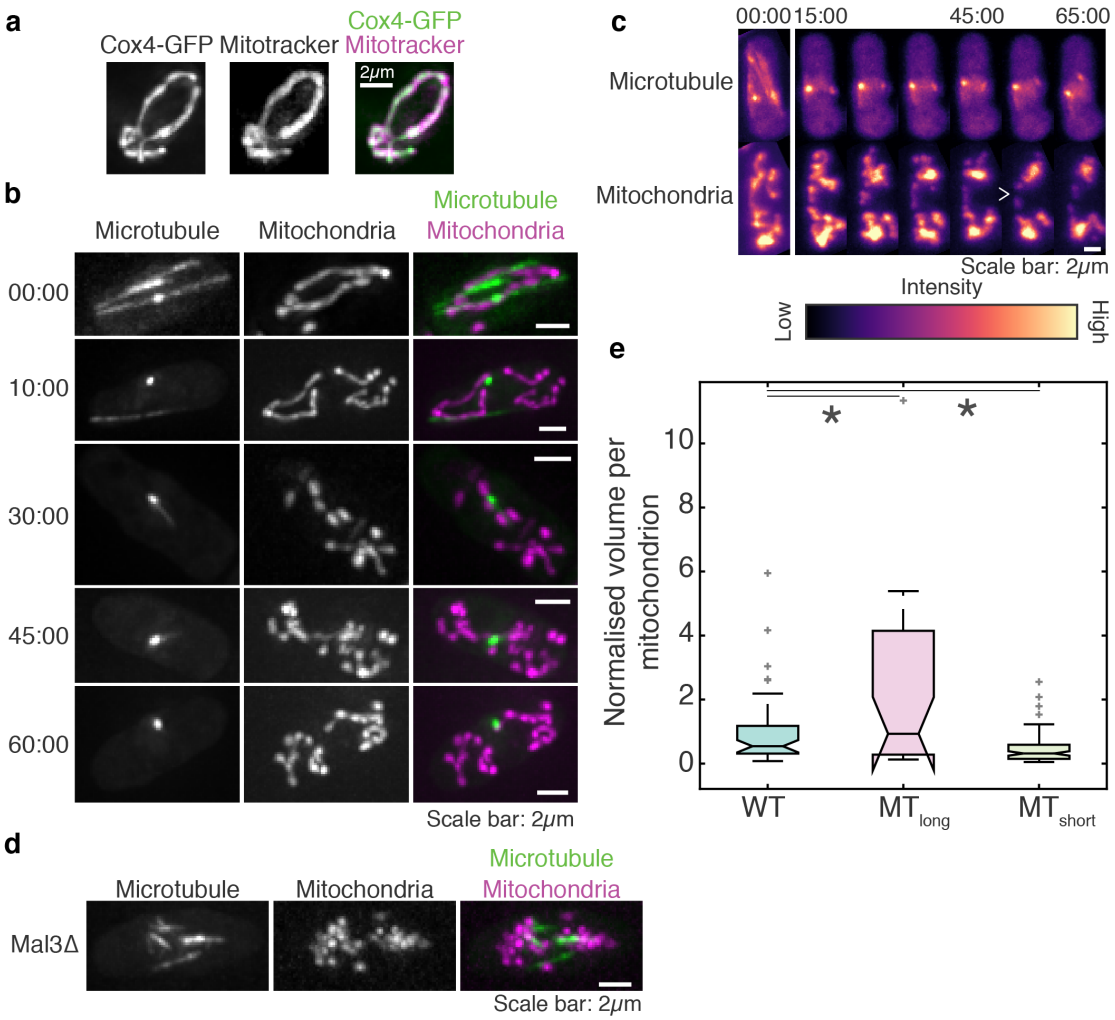

Extended Data Figure 1. Depolymerisation of microtubules increases mitochondrial fission. a, Maximum intensity projections of deconvolved Z-stack images of Cox4-GFP (left), Mitotracker Orange staining (centre) and their composite (right) in interphase cells (strain PT.1650, see Table S1) showing colocalisation of both signal intensities. **b,** Maximum intensity projections of deconvolved Z-stack images of microtubules (left), mitochondria (centre) and their composite (right) in fission yeast cells at the onset of mitosis. Time in mm:ss is indicated to the left of the images. **c,** Montage of maximum intensity projected confocal Z-stack images of microtubule depolymerisation (top) and mitochondria (bottom) of wild-type cells (strain KI001, see Table S1) treated with MBC (see Supplementary Information) represented in the intensity map indicated at the bottom of the images. The open white arrowhead indicates a representative fission event. **d,** Box plot of the volume of individual mitochondria in wild-type ('WT'), Klp5Δ/Klp6Δ ('MT_{long}') and Klp4Δ ('MT_{short}') cells normalised to mean mitochondrial volume in wild-type cells (n=49, 28 and 100 mitochondria respectively). Light grey crosses represent outliers, asterisk represents significance ($p<0.05$) and 'n.s.' indicates no significant difference. **e,** Maximum intensity projections of deconvolved Z-stack images of microtubule (left), mitochondria (centre) and their composite (right) in interphase Mal3Δ cells (strain KN001, see Table S1) showing several small mitochondrial fragments similar to those seen in Klp4Δ cells.

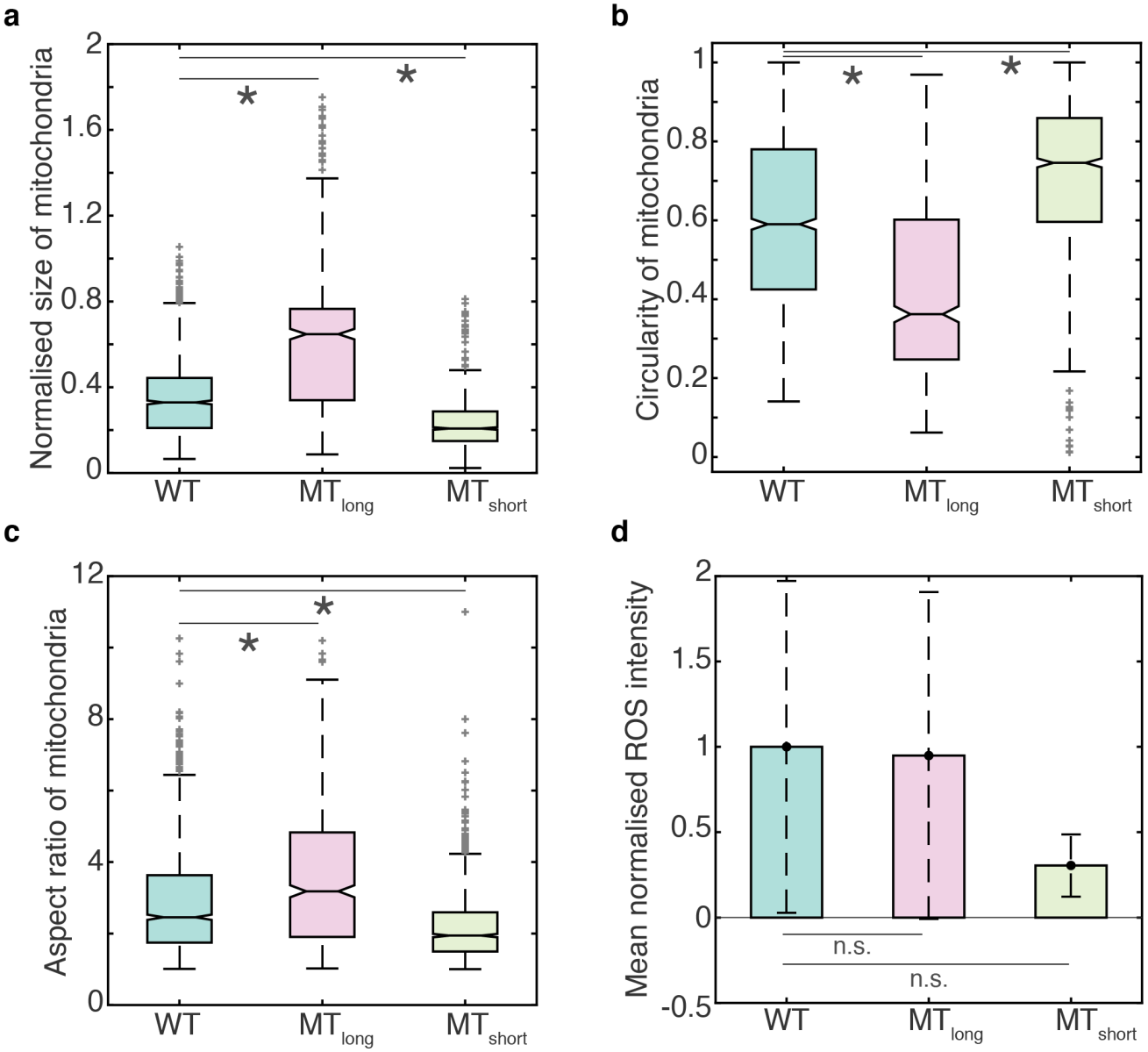

Extended Data Figure 2. Microtubule dynamics determines the morphology of mitochondria. a, Box plot of the size of individual mitochondria in wild-type ('WT'), Klp5Δ/Klp6Δ ('MT_{long}') and Klp4Δ ('MT_{short}') cells normalised to their cell lengths (*n*=1613, 739 and 1326 mitochondria respectively). **b,** Box plot of the circularity of mitochondria in WT, MT_{long} and MT_{short} cells (*n*=1613, 739 and 1326 mitochondria respectively). **c,** Box plot of the aspect ratio of mitochondria in WT, MT_{long} and MT_{short} cells (*n*=1613, 739 and 1326 mitochondria respectively). **d,** Bar plot of cellular ROS measured using flow cytometry (see Supplementary Information) in live WT, MT_{long} and MT_{short} cells normalised to mean of the ROS intensity in WT cells (*n*=3 independent experiments, ≥10,000 events each). Error bars represent standard deviation. Light grey crosses represent outliers, asterisk represents significance ($p<0.05$) and 'n.s.' indicates no significant difference

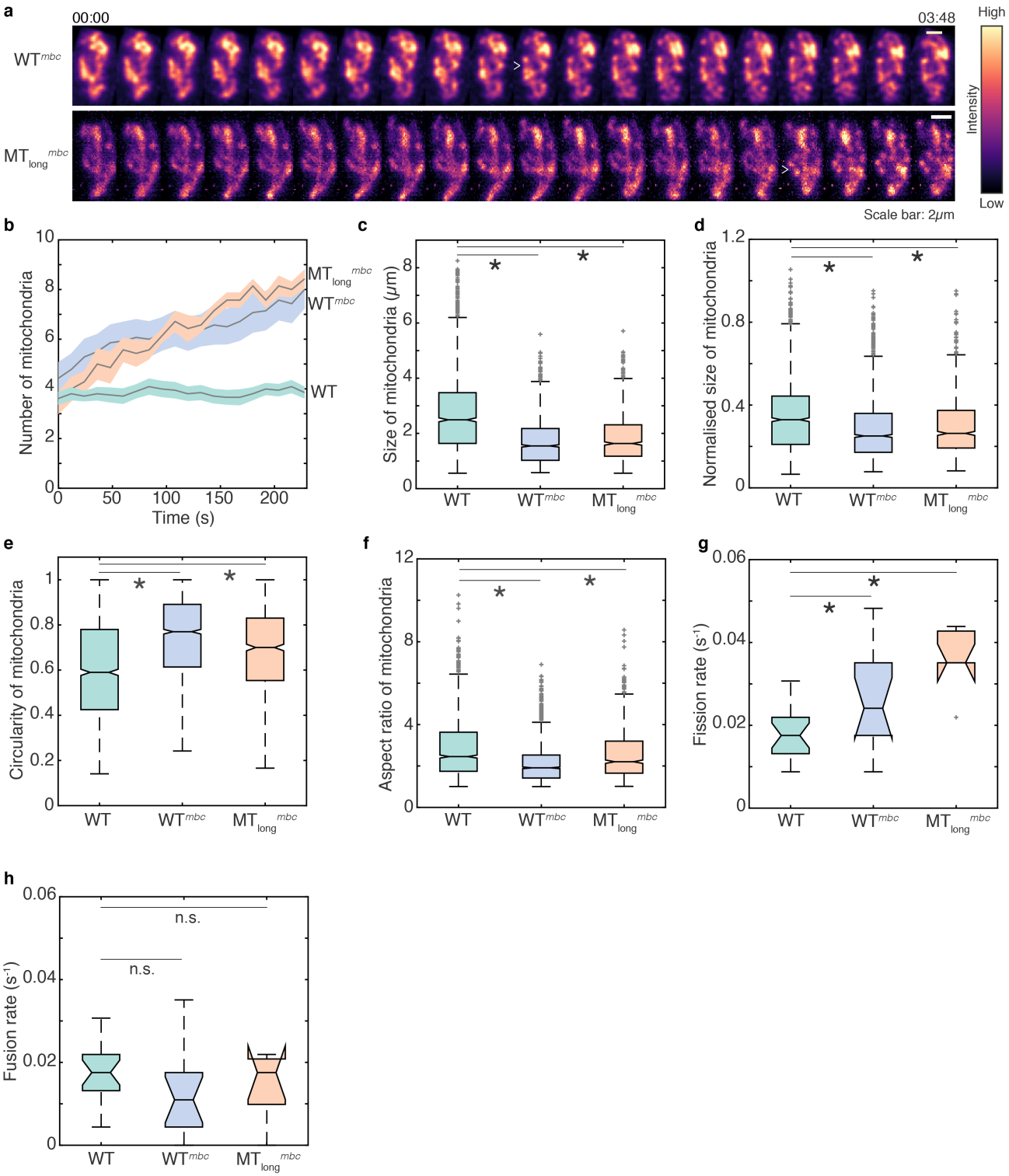

Extended Data Figure 3. Microtubule depolymerisation induces increased fission in Klp5Δ/Klp6Δ cells. a, Montage of maximum intensity projected confocal Z-stack images of MBC-treated wild-type (WT^{mbc}, strain KI001, see Table S1) and Klp5Δ/Klp6Δ ('MT_{long}^{mbc}', strain G3B, see Table S1) cells represented in the intensity map indicated to the right of the images. White open arrowheads point to representative fission events. 00:00 indicates time (mm:ss) 2min after addition of MBC. **b,** Evolution of mitochondrial number with time indicated as mean (solid grey line) and standard error of the mean (shaded region) for wild-type ('WT'), WT^{mbc}, and MT_{long}^{mbc} cells (n=21, 14 and 7 cells respectively). **c,** Box plot of the size of mitochondria in WT, WT^{mbc}, and MT_{long}^{mbc} cells, calculated as the length of the major

axis of an ellipse fitted to each mitochondrion (*n*=1613, 1765 and 886 mitochondria respectively). **d,** Box plot of the size of individual mitochondria in WT, WT^{mbc}, and $MT_{long}{}^{mbc}$ cells normalised to their cell lengths (*n*=1613, 1765 and 886 mitochondria respectively). **e,** Box plot of the circularity of mitochondria in WT, WT^{mbc}, and $MT_{long}{}^{mbc}$ cells (*n*=1613, 1765 and 886 mitochondria respectively). **f,** Box plot of the aspect ratio of mitochondria in WT, WT^{mbc}, and $MT_{long}{}^{mbc}$ cells (*n*=1613, 1765 and 886 mitochondria respectively). **g,** Box plot of the fission rate of mitochondria per second in WT, WT^{mbc}, and $MT_{long}{}^{mbc}$ cells (*n*=21, 14 and 7 cells respectively). **h,** Box plot of the fusion rate of mitochondria per second in WT, WT^{mbc}, and $MT_{long}{}^{mbc}$ cells (*n*=21, 14 and 7 cells respectively). Light grey crosses represent outliers, asterisk represents significance ($p<0.05$) and 'n.s.' indicates no significant difference. Note that the WT data represented in this figure is the identical to the wild-type data plotted in Fig. 2 and Extended Data Fig. 2 and has been re-used for comparison.

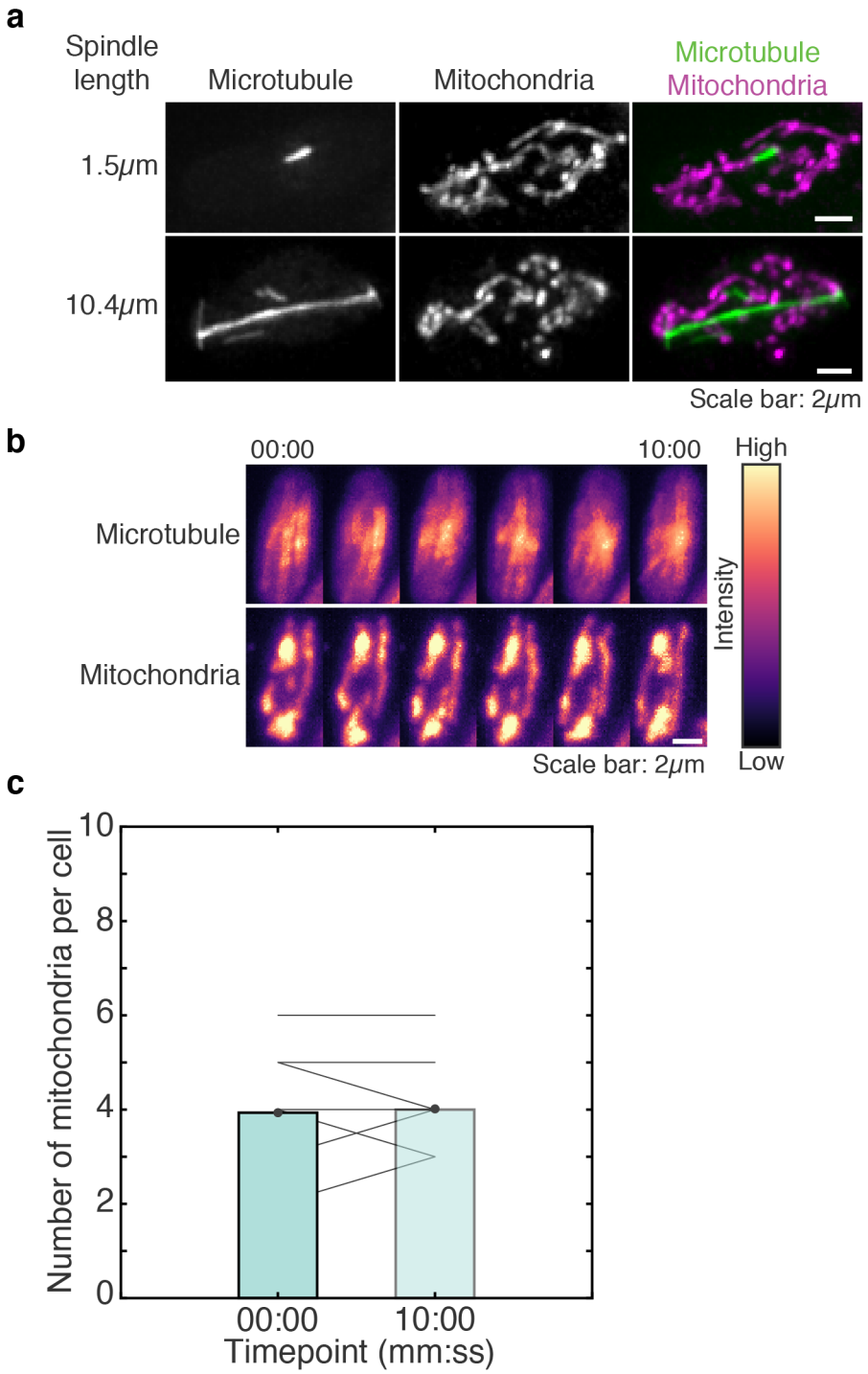

Extended Data Figure 4. Mitotic spindle length does not influence number of mitochondria. a, Maximum intensity projections of deconvolved Z-stack images of the microtubules (left), mitochondria (centre) and their composite (right) of WT cells (strain KI001, see Table S1) with short (top) and long (bottom) mitotic spindles. The length of the spindle is indicated to the left of the images. **b,** Montage of maximum intensity projected confocal Z-stack images of the microtubules (top) and mitochondria (bottom) in a non-mitotic wild-type cell (strain KI001, see Table S1) represented in the intensity map indicated to the right of the images.. **c,** Bar plot of the mean number of mitochondria per cell before ('00:00') and after ('10:00') the same time window for which mitotic cells were monitored in Fig. 3c, d. Solid grey lines represent data from individual cells (*n*=7 cells).

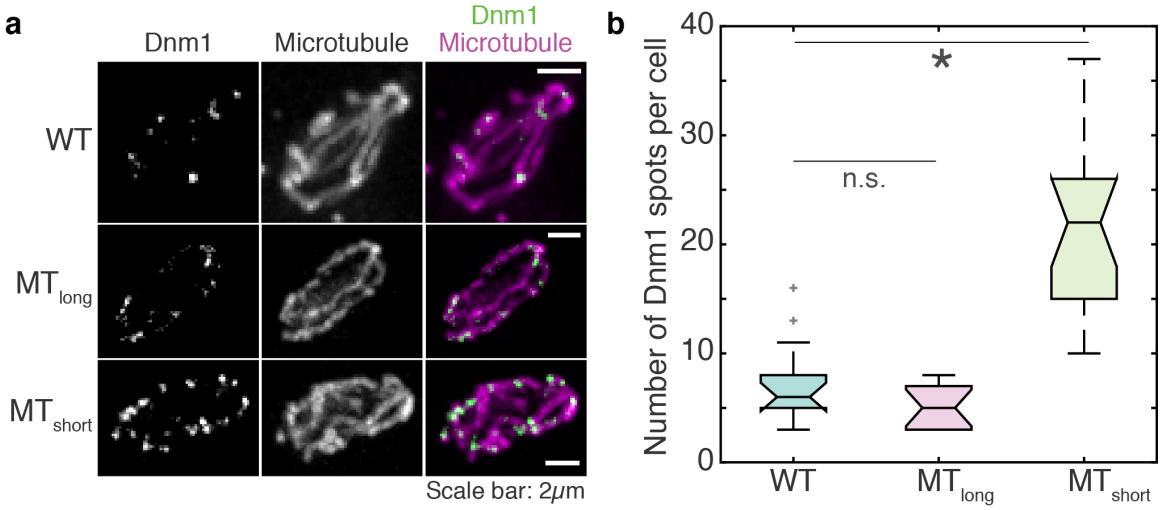

c

Parameter	Value (mean ± s.e.m)		
	WT	MT_{long}	MT_{short}
Number of mitochondria	4.9 ± 0.4	2.3 ± 0.4	10 ± 0.9
Normalised total volume of mitochondria	1.00 ± 0.10	1.09 ± 0.13	0.92 ± 0.07
Normalised volume of individual mitochondria	1.00 ± 0.16	2.30 ± 0.50	0.45 ± 0.04
Size of mitochondria (μm)	2.72 ± 0.03	6.53 ± 0.11	1.77 ± 0.02
Size of mitochondria normalised to cell length	0.35 ± 0.01	0.59 ± 0.01	0.23 ± 0.01
Circularity of mitochondria	0.60 ± 0.01	0.44 ± 0.01	0.71 ± 0.01
Aspect ratio of mitochondria	2.84 ± 0.04	3.55 ± 0.07	2.16 ± 0.03
Mitochondrial fission rate (s^{-1})	0.018 ± 0.002	0.006 ± 0.001	0.032 ± 0.005
Mitochondrial fusion rate (s^{-1})	0.017 ± 0.002	0.011 ± 0.001	0.025 ± 0.005

Extended Data Figure 5. Dnm1 spots colocalise with the mitochondria and their number is inversely proportional to the length of microtubules. a, Maximum intensity projections of deconvolved Z-stack images of Dnm1 (left), microtubules (centre) and their composite (right) in wild-type ('WT', strain FY7143 transformed with pREP41-Dnm1-Cterm-GFP, see Table S1), Klp5Δ/Klp6Δ ('MT_{long}', strain FY20832 transformed with pREP41-Dnm1-Cterm-GFP, see Table S1) and Klp4Δ ('MT_{short}', strain Mcl438 transformed with pREP41-Dnm1-Cterm-GFP, see Table S1) cells. **b,** Box plot of the number of Dnm1 spots in WT, MT_{long} and MT_{short} cells (n=13, 14, and 18 cells respectively). Note that the mitochondrial morphology in WT, MT_{long} and MT_{short} cells appears abnormal due to inactivity of the GFP-tagged Dnm1. Light grey crosses represent outliers, asterisk represents significance ($p<0.05$) and 'n.s.' indicates no significant difference **c,** Measured parameters relating to mitochondrial numbers and morphology in WT, MT_{long} and MT_{short} interphase cells represented as mean ± s.e.m.

Supplementary Information

METHODS

Strains and media. The fission yeast strains used in this study are listed in Table S1. All the strains were grown in YE (yeast extract) media or Edinburg Minimal media (EMM)[1] with appropriate supplements at a temperature of 30˚C. Cells that were transformed with pREP41-Dnm1-Cterm-GFP (see below) were cultured in EMM with appropriate supplements and 0.05μM thiamine for partial induction of the nmt1 promoter.

Plasmid transformation. Transformation of strains MTY271, FY7143, FY20823 and Mcl438 with plasmid pREP41-Dnm1-Cterm-GFP (see Table S1) was carried out using the improved protocol for rapid transformation of fission yeast[2]. In brief, cells were grown overnight to log phase in low glucose EMM, pelleted and washed with distilled water. The cells were then washed in a solution of lithium acetate/EDTA (100mM LiAc, 1mM EDTA, pH 4.9) and re-suspended in the same solution. 1μg of plasmid DNA was added to the suspension, followed by addition of lithium acetate/PEG (40% w/v PEG, 100mM LiAc, 1mM EDTA, pH 4.9) and then incubated at 30°C for 30 min. This was followed by a heat shock of 15min at 42°C. Thereafter, cells were pelleted down, re-suspended in TE solution (10mM Tris-HCl, 1mM EDTA, pH 7.5) and plated onto selective EMM plates.

Preparation of yeast for imaging. For imaging mitochondria, fission yeast cells were grown overnight in a shaking incubator at 30°C, washed once with distilled water, and stained with 200nM Mitotracker Orange CMTMRos (ThermoFisher Scientific, Cat. #M7510) dissolved in EMM for 20min. Following this, cells were washed thrice with EMM and then allowed to adhere on lectin-coated (Sigma-Aldrich, St. Louis, MO, Cat. #L2380) 35mm confocal dishes (SPL, Cat. #100350) for 20min. Unattached cells were then removed by washing with EMM. In experiments where mitochondria were not imaged, staining with Mitotracker was omitted.

Microtubule depolymerisation. For depolymerisation of microtubules, cells were treated with methyl benzimidazol-2-yl-carbamate (MBC, Carbendazim 97%, Sigma Aldrich). A stock solution with a concentration of 25mg/ml was prepared in DMSO and later diluted to a working concentration of 25μg/ml in EMM.

ROS detection and viability assay using flow cytometry. A loopful of L972, FY20832 or Mcl438 cells were inoculated in liquid YE and incubated overnight at 30°C in a shaking incubator. Cells were harvested using a table-top centrifuge (2000g, 30s) and washed three times with 1X PBS. The pellets were re-suspended in 500μl of 1X PBS, containing CellROX (5μM) dye (ThermoFisher, USA). Following incubation at 30°C for 30min, cells were washed three times with 1X PBS. Finally, cell pellets were re-suspended in an appropriate volume of 1X PBS containing propidium iodide (6μg/ml), incubated for 10min at room temperature, and run on a flow cytometer (BD FACS-Celesta). A minimum of 10,000 events of cells was collected, and data analyzed using FlowJo (FlowJo LLC, USA). ROS was reported as median fluorescence intensity for each dataset.

Microscopy. Confocal microscopy was carried out using the InCell Analyzer-6000 (GE Healthcare, Buckinghamshire, UK) with 60x/0.7 N.A. objective fitted with an sCMOS 5.5MP camera having an x-y pixel separation of 108nm. For GFP and Mitotracker Orange imaging,

488 and 561nm laser lines and bandpass emission filters 525/20 and 605/52nm respectively were employed. Time-lapses for visualisation of mitochondrial dynamics were captured by obtaining 5 Z-stacks with a 0.5μm-step size every 12s. Deconvolution was performed in images obtained using a Deltavision RT microscope (Applied Precision) with a 100×, oil-immersion 1.4 N.A. objective (Olympus, Japan). Excitation of fluorophores was achieved using InsightSSI (Applied Precision) and corresponding filter selection for excitation and emission of GFP and Mitotracker Orange. Z-stacks with 0.3μm-step sizes encompassing the entire cell were captured using a CoolSnapHQ camera (Photometrics), with 2X2 binning. The system was controlled using softWoRx 3.5.1 software (Applied Precision) and the deconvolved images obtained using the built-in setting for each channel.

3D visualisation of deconvolved images. 3D views of the microtubules and mitochondria in Supplementary Movies S2, S3, S4, S8 and S9 were obtained from deconvolved images captured in the Deltavision microscope using Fiji's '3D project' function, with the brightest point projection method and 360˚ total rotation with 10˚ rotation angle increment.

Estimation of volume of mitochondria. Mitochondrial volume was estimated in Fiji by integrating the areas of mitochondria in thresholded 3D stacks of cells in fluorescent deconvolved images obtained using the Deltavision RT microscope. The total volume was then normalised to the mean total mitochondrial volume of wild-type cells. Individual mitochondrial volumes were estimated in the same fashion.

Analysis of mitochondrial dynamics. Individual mitochondria were identified in each frame of the time-lapse obtained in confocal mode of the GE InCell Analyzer after projecting the maximum intensity of the 3D stack encompassing the cell, followed by mean filtering and visualisation in Fiji's 'mpl-magma' lookup table. Following identification of mitochondria, the 'Measure' function of Fiji was employed to obtain the circularity, aspect ratio and parameters of fitted ellipse. The length of the major axis of the ellipse fitted to a mitochondrion was defined as the size of that mitochondrion. The size, circularity and aspect ratio were estimated for mitochondria at each frame and each time point. Fission and fusion rates of mitochondria were estimated by counting the number of mitochondria identified during each frame of the time-lapse. The difference in number of mitochondria from one frame to the next was counted, with an increase being counted as fission event and decrease as fusion event. The total number of fission events and fusion events per cell were estimated and divided by the total duration of the time-lapse to obtain the fission and fusion rates.

Counting of Dnm1 spots. Dnm1 was visualised in cells grown in the presence of 0.05μM thiamine for partial induction of the nmt1 promoter. Even with only partial induction, a majority of the cells showed extremely high expression of Dnm1, with most of the signal concentrated in a single spot in the cell. The rest of the cells showed lower expression, with Dnm1 signal distributed in a few spots across the cell. The latter were chosen for analysis of number of Dnm1 spots. For counting the number of Dnm1 spots in Extended Data Fig. 5b, the maximum intensity projection of deconvolved Z-stack images were used. For identification of spots, we set the lower threshold as 60-80% of the maximum intensity in these images. The contrast in the images in Fig. 4a and Extended Fig. 5a reflect these threshold settings.

Data analysis and plotting. Data analysis was performed in Matlab (Mathworks, Natick, MA). Box plots with the central line indicating the median and notches that represent the 95% confidence interval of the median were obtained by performing one-way ANOVA ('anova1' in Matlab). Following this, significance ($p<0.05$) of the means was tested using the Tukey-Kramer post-hoc test. All the plots were generated using Matlab.

Supplementary References

1. Forsburg, S. L. & Rhind, N. Basic methods for fission yeast. *Yeast* **23,** 173–183 (2006).
2. Kanter-Smoler, G., Dahlkvist, A. & Sunnerhagen. Improved Method for rapid Transformation of Intact Schizosaccharomyces pombe cells. *Biotechniques* **16,** 798–800 (1994).

Table S1

Strains and constructs used in this study

Name	Phenotype	Source
FY20823	*h- leu1 ura4 his7 Δklp5::ura4+ Δklp6::ura4+*	NBRP, Japan
FY7143	*h- ura4-D18 leu1-32 ade6-M216 his7-366*	Iva Tolić, Croatia
G3B	*h- Δklp5- Δklp6 – nmt1-GFP-atb2 leu ade*	Rafael Carazo Salas, UK
G5B	*h- klp4::kanr nmt1-GFP-atb2 leu ura*	Rafael Carazo Salas, UK
KI001	*h+ sid4-GFP::kanr kanr -nmtP3-GFP-atb2+ nmt1-pCOX4RFP::leu1+ ura4-D18 ade6-M210*	Iva Tolić, Croatia
KN001	*h + Δmal3::his3+ nmt1-pCOX4-dsRed ::leu1+ nmt1-atb1-GFP:LEU2 ade6-M210 ura4-D18 leu1-32 his3D1*	Iva Tolić, Croatia
L972	*h- WT*	Iva Tolić, Croatia
McI438	*h+ tea2d:his3 ade6 leu1-32 ura4-D18 his3-D1*	Iva Tolić, Croatia
MTY271	*h- mCherry-atb2:hphMX6 leu1-32 ura-d18*	Masakatsu Takaine, Japan
PT1650	*h+ cox4-GFP:leu1 ade6-M210 leu1-32 ura4-D18*	Phong Tran, USA
pREP41-Dnm1-Cterm-GFP (plasmid)	*Dnm1-GFP*	Isabelle Jourdain, UK

Supplementary video captions

Video S1. Live-cell confocal microscopy of MBC-treated interphase fission yeast cells with the mitochondria stained with Mitotracker. Warmer colours indicate higher intensities. Images were acquired at 2min intervals. Time 00:00 (mm:ss) indicates time of addition of MBC. Imaging was resumed 15min after MBC addition ('15:00'). Scale bar represents 2μm. This movie corresponds to Extended Data Fig. 1c.

Video S2. 3D projection of microtubules (green) and mitochondria (magenta) in a wild-type cell (strain KI001, see Table S1). This movie corresponds to Fig. 1a.

Video S3. 3D projection of microtubules (green) and mitochondria (magenta, stained with Mitotracker) in a Klp5Δ/Klp6Δ cell (strain G3B, see Table S1). This movie corresponds to Fig. 1a.

Video S4. 3D projection of microtubules (green) and mitochondria (magenta, stained with Mitotracker) in a Klp4Δ cell (strain G5B, see Table S1). This movie corresponds to Fig. 1a.

Video S5. Mitochondrial dynamics in a wild-type cell (strain KI001, see Table S1) stained with Mitotracker. A 5-slice Z-stack with step size of 0.5μm was obtained every 12s. The video represents the maximum-intensity projected images of the stacks obtained. Warmer colours indicate higher intensity. The closed white arrowhead points to a fusion event and the open white arrowhead points to a fission event. Scale bar represents 2μm. This movie corresponds to Fig. 2a.

Video S6. Mitochondrial dynamics in a Klp5Δ/Klp6Δ cell (strain G3B, see Table S1) stained with Mitotracker. A 5-slice Z-stack with step size of 0.5μm was obtained every 12s. The video represents the maximum-intensity projected images of the stacks obtained. Warmer colours indicate higher intensity. The closed white arrowhead points to a fusion event. Scale bar represents 2μm. This movie corresponds to Fig. 2a.

Video S7. Mitochondrial dynamics in a Klp4Δ cell (strain G5B, see Table S1) stained with Mitotracker. A 5-slice Z-stack with step size of 0.5μm was obtained every 12s. The video represents the maximum-intensity projected images of the stacks obtained. Warmer colours indicate higher intensity. The open white arrowhead points to a fission event. Scale bar represents 2μm. This movie corresponds to Fig. 2a.

Video S8. 3D projection of microtubules (green) and mitochondria (magenta) in a wild-type mitotic cell (strain KI001, see Table S1). This movie corresponds to Fig. 3a.

Video S9. Microtubule dynamics (left) and mitochondrial dynamics (right) in a wild-type cell (KI001, see Table S1) at the onset of mitosis. A 5-slice Z-stack with step size of 0.5μm was obtained every 2min. The video represents the maximum-intensity projected images of the stacks obtained. Warmer colours indicate higher intensity. Scale bar represents 2μm. The open white arrowheads point to fission events. This movie corresponds to Fig. 3b.

Video S10. 3D projection of Dnm1 (green) and microtubules (magenta) in wild-type cells (strain MTY271 transformed with pREP41-Dnm1-Cterm-GFP, see Table S1). This movie corresponds to Fig. 4a.